Why do you get the cold in the winter? Developing a temperature-dependent kinetic model for human rhinovirus infection

Authors:

Page Murray

Mia Pergola

Andrew Sweatt

Kevin Janes

Words: 5680

Number of Figures: 6

Number of Tables: 0

Number of Equations: 2

Number of Supplements: 5

Number of References: 25

Why do you get the cold in the winter? Developing a temperature-dependent kinetic model for human rhinovirus infection.

Page C. Murray[a], Mia C. Pergola[a], Andrew Sweatt[a], Kevin A. Janes[b,1]

[a] Biomedical Engineering, University of Virginia
[b] Microbiology, Immunology, and Cancer Biology, University of Virginia
[1] Correspondence: K.A.J
Email: kjanes@virginia.edu
Address: Box 800759, Health System, Charlottesville, VA 22908
Phone: 434-982-3870

Abstract

Human Rhinovirus (HRV) causes the common cold and represents a significant disease burden annually. HRV paradoxically produces more virions at 33℃ than 37℃, which is counterintuitive because kinetic and thermodynamic rates slow down at lower temperatures. To investigate a mechanistic explanation of the temperature-dependent virion production in HRV infection, we adapted a complete kinetic model that has been previously used to study related viruses. Accurate modeling of viral capsid formation is essential to capture temperature-dependent behavior because capsid assembly is a thermodynamic process. Kinetic and thermodynamic temperature-dependence were incorporated throughout the model and model assumptions concerning capsid formation were reevaluated. These model modifications revealed the documented temperature-dependent behavior. We show that kinetic temperature-dependence is essential to reveal model predictions of higher virion production at lower temperatures. Additionally, changing the model assumptions for capsid assembly to detail the kinetics of capsid assembly is necessary for the model predictions to agree with the observed temperature-dependence of HRV. Our model predicts that early peaks in viral intermediates at 37℃ in comparison to 33℃ lead to rate imbalances that cause lower virion production. Our model raises the possibility that the unusual temperature-dependent behavior of HRV may stem from imbalances in viral intermediate production and consumption within viral replication and capsid formation.

Key words: enterovirus, picornavirus, Arrhenius equation, Van't Hoff equation, viral encapsidation, viral pentamers

Introduction

Enteroviruses are a genus of non-enveloped, single-stranded, positive-sense RNA viruses that are among the most common pathogens worldwide, causing complications ranging from heart conditions like myocarditis to hepatitis[1–3]. Human rhinovirus (HRV) is a member of the enterovirus genus[3]. It is associated with upper respiratory tract infection, middle ear infection, sinus infections, the common cold and bronchitis[3,4]. Specifically, HRV is responsible for more than half of cold-like illnesses annually. This poses a significant risk to the health of immunocompromised individuals, the elderly, infants, and patients with chronic respiratory diseases[4]. In 2015, HRV was responsible for over 700 hospitalizations[5]. In addition to the health risks, it also represents a significant economic strain as it is estimated that roughly $40 billion is spent annually on non-influenza virus respiratory tract infections caused by HRV[4].

HRV has been shown to produce virions more rapidly at 33°C than at 37°C[6]. This finding is unexpected because low temperatures will decrease kinetic rates, which would be expected to decrease viral propagation. Biologists have rationalized this behavior from an evolutionary standpoint—HRV infects the nasal cavity, which is typically at a temperature of approximately 33°C[7,8]; therefore, HRV has evolved to increase production at this temperature. However, this does not mechanistically explain why virion production would be greater at a lower temperature when compared to higher temperature. Thus, our capstone investigated possible mechanistic explanations

for this behavior through the adaptation of a published complete kinetic model.

Having a clear understanding of the viral mechanisms, involving delivery, replication, and encapsidation, is essential to the development of effective therapeutics to treat HRV. Computational models facilitate research by allowing investigators to test ideas without having to use time-consuming cellular or mouse models. For example, the development of an Influenza A kinetic model led to identification of certain membrane proteins as rate limiting factors[9,10]. Additionally, Coxsackievirus models have identified genetic mutations as predictors of the strength of the innate immune response[11]. The development of a compartment model for HRV infection that contains detailed viral mechanisms will offer greater insight into the kinetics of this process by predicting the concentrations of viral intermediates overtime. A model of HRV can be similarly used to identify genes of interest to predict patient outcomes. Moreover, given that HRV is a member of the enterovirus genus, the model of HRV will lead to a better understanding of the enterovirus genus as a whole.

Previously, our lab developed a MATLAB model of Coxsackievirus B3, an enterovirus implicated in the development of myocarditis among infants. This model separates the viral life cycle into three modules—viral delivery, viral replication, and viral encapsidation—with the innate immune response overlaid at various points in the life cycle. The model predicts multiple outputs including the quantities of viral RNA, viral protein, virions released, and interferon-stimulated genes produced in response to viral infection. This model constitutes a 'complete kinetics' model[11]. Complete kinetics refers to a structural model where the viral life cycle is stoichiometrically represented as a sequence of well characterized reactions. The innovative use of this mathematical model for biological processes involves explicitly defined reactants and products, the inclusion of catalysts, and mass balancing, which, all together, provide for a much more mechanistic and detailed understanding of viral infection. Complete kinetics also allows for improved modularity of the various features. Because each step is separated from the next, one step can be changed to reflect a new virus without having to change the entire model. Specific receptor binding archetypes can be swapped out for one another to allow for rapid adaptation of the model. This complete structural model is a useful method of investigating uncharacterized viral behavior.

To study HRV, we adapted the existing CVB3 model to HRV by altering the delivery module architecture to reflect HRV binding interactions. Moreover, the unique temperature-dependent behavior of HRV is not accounted for in the original CVB3 model[6]. Therefore, temperature-dependence was incorporated into the entirety of the new model through both kinetic and thermodynamic equations. We hypothesized that thermodynamic equilibriums create an imbalance between the amount of viral RNA and capsids in the encapsidation process. The CVB3 model simplifies the complicated mechanism of encapsidation by lumping parameters into a single kinetic parameter due to lack of available data. To investigate the importance of thermodynamic temperature-dependence in encapsidation, we reevaluated the simplification within the encapsidation process to provide a more mechanistically detailed explanation of encapsidation. The MATLAB model for HRV shows that incorporating kinetic temperature-dependence and desimplification of encapsidation reveals the documented result of more virion production at 33℃ compared to 37℃. Model predictions suggest that the unusual temperature-dependent behavior of HRV is mechanistically possible due to imbalances in viral intermediate production with regards to viral protease activity and capsid formation.

Results

Adaption of previous model to HRV

To model HRV infection, a previous model of CVB3 was adapted to HRV (Figure 1A). Because HRV and CVB3 are closely related viruses, only the cell entry steps, represented in the delivery module, differ between the two viruses (Figure 1B). HRV has a quicker and simpler delivery module as it has only one receptor that it binds to with a higher affinity than CVB3 binds its receptor. To model HRV, HRV2 and HRV3 were chosen to represent the minor and major serotypes respectively. HRV2 binds low density lipoprotein receptor (LDLR) at one site, while HRV3 binds intercellular adhesion molecule (ICAM1) at two sites. New rate parameters were taken from the literature for HRV2 and HRV3, and the model architecture was restructured to match either HRV2 or HRV3 delivery (Figure 1B). This resulted in two separate versions of the HRV model. The two versions of the HRV model were compared to the previous CVB3 model using the model predictions of virions produced over infection. HRV infection begins quickly, with virions appearing between 3–4 hours, while virions appear between 5–6 hours in CVB3 infection (Figure 2). This was expected due to the simpler delivery module architecture in HRV and faster rate of

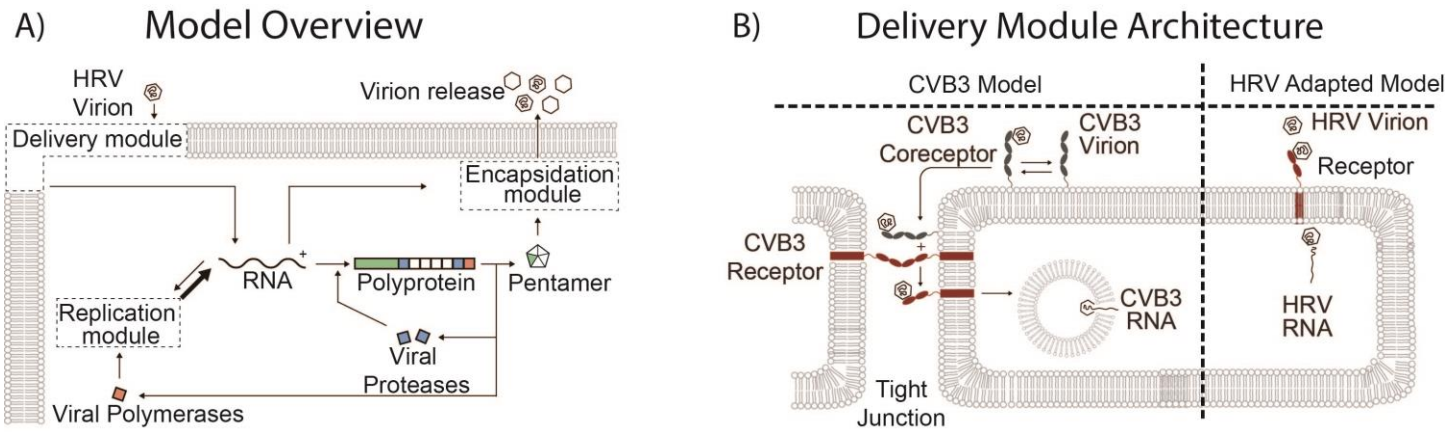

Figure 1: A) Overview of the HRV model architecture. HRV enters through a module of receptors and trafficking states that delivers its positive-strand RNA genome to the cytoplasm. RNA is translated into a polyprotein that is cleaved into capsid monomers contributing one fifth of a pentamer of a 12-pentamer capsid, viral proteases, and RNA-dependent RNA polymerase 3D. Polymerase 3D replicates positive sense RNA through a negative-strand intermediate in a module that gives rise to excess positive sense RNA, which joins with pentamer in an encapsidation module that self-assembles pentamers around positive sense RNA and leads to virion release. B) Comparison between CVB3 delivery and HRV delivery. CVB3 binds its coreceptor, translocates into the tight junction to bind its receptor and is then internalized via endocytosis. HRV binds to its receptor and is internalized by many separate mechanisms that are modeled as a single rate. Rates comparing CVB3 and HRV delivery module rates are available in supplementary table 1.

internalization in comparison to CVB3 (Figure 1B, S1). CVB3 infection surpasses HRV infection at the 7-hour timepoint. This can be explained by fast internalization leading to imbalances in the production and consumption of viral intermediates. Specifically, viral polymerase and viral pentamers peak earlier in HRV infection. These two species have then disappeared later in HRV infection, at the same time points that CVB3 viral polymerase and viral pentamers reach their peak. The difference between HRV2 and HRV3 was less than 2% at all time points. Because the difference in model predictions between HRV2 and HRV3 were so slight, HRV2 will be focused on for simplicity in the remainder of this paper. The described results were compared to various data points taken from the literature including appearance of virions in cell media and appearance of negative single stranded RNA in the lysate[12–14]. This verification gives confidence that the model architecture is accurately modeling HRV infection.

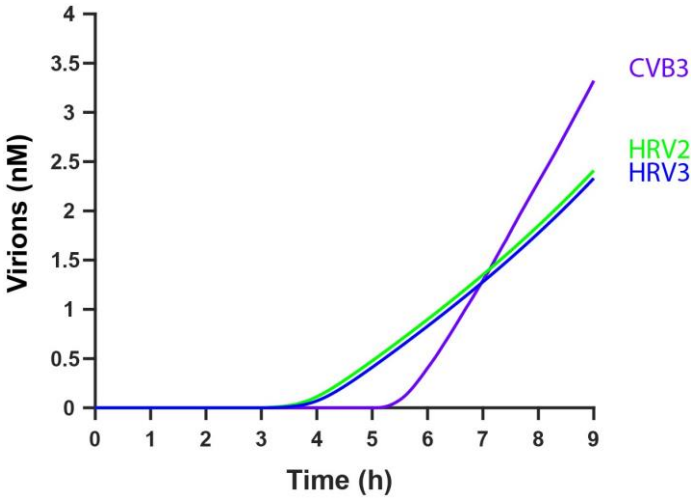

Figure 2: Comparison of virion production over time between CVB3, HRV2 and HRV3. All infections were simulated 100 times with a multiplicity of infection (MOI) of 10. The solid lines represent the median simulation of each condition.

Incorporation of kinetic and thermodynamic temperature-dependence

After the model architecture had been adapted to HRV infection, temperature-dependence was incorporated into the model (Figure 3). This was done either using kinetics with the Arrhenius equation (Equation 1) or thermodynamics with the Van't Hoff equation (Equation 2). The Arrhenius equation was used to model kinetic temperature-dependence in the delivery and replication modules, where catalytic processes are important for infection. We used this equation to recalculate the kinetic rate constant at 33℃. This required finding activation energies for parameters within these modules. In cases where activation energies were unknown, we defined a range of biologically plausible activation energies. The Van't Hoff equation was used in the encapsidation module where thermodynamic self-assembly drives viral behavior. Our goal was to recalculate the affinity constant at 33℃. To do so, a range of biologically plausible enthalpies were encoded into the model (see Materials & Methods). The model was run for approximately 3,000 simulations, so as to cover a large sample of possible combinations of activation energy and enthalpy values. Each simulation

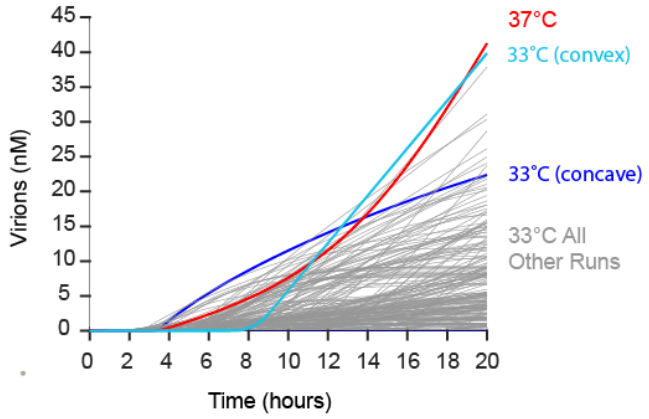

Figure 3: Effect of temperature-dependence on HRV model predictions. Temperature-dependence was incorporated using both the Arrhenius equation and the Van't Hoff equation. The model was run for 3,000 simulations with an MOI of 10. The grayed-out lines represent simulations run at 33°C that were not of interest as resulted in lower virion concentration predictions. This is an example of a single column figure.

represented a different combination of activation energies and enthalpies for the unknown model parameters in an effort to determine if any combinations resulted in the observed behavior of greater virion production at 33°C than 37°C. The run at 37°C represented the result of all 3,000 simulations; however, since all the rate constants were originally defined at 37°C, all model simulations at this temperature were identical regardless of activation energy and enthalpy values chosen for the unknown parameters. We have highlighted two representative instances out of the 3,000 simulations where the model predictions at 33°C surpassed those at 37°C (Figure 3). The two different curve types (concave and convex) at 33°C are likely attributable to the rand of both negative and positive enthalpy values possible in the model.

The convex curve at 33°C starts off at approximately the 8-hour time point whereas the 37°C curve starts off at 3–4 hours. Despite having a steeper slope, the 33°C has a slightly lower virion production at the end point of 20 hours where viral infection has gone to completion. The concave curve at 33°C starts at the same point as the 37°C curve; however, it begins increasing faster. Therefore, at early time points, the concave 33°C curve has higher virion production than at 37°C. However, virion production predicted by the concave 33°C curve rapidly slows down, enabling the 37°C curve to pass the 33°C curve at a time point of approximately 14 hours.

Neither the convex nor the concave curve at 33°C results in the expected model behavior. The literature reports a large increase in virion concentration at 33°C

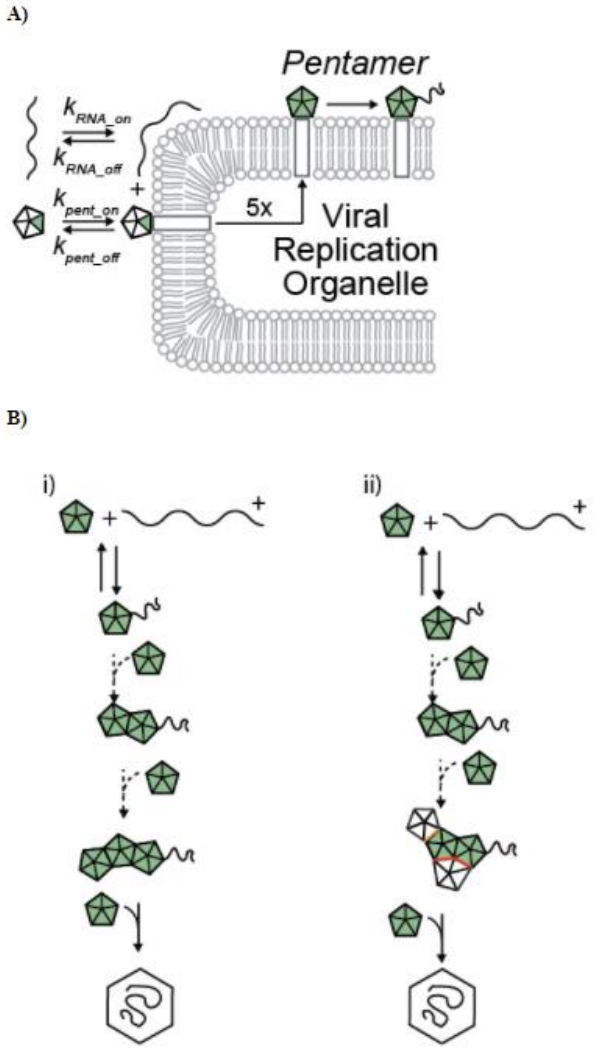

Figure 4: Explanation of encapsidation. A) diagram of pentamer formation. Individual protomers (green triangles) associate with the viral replication organelle (VRO). Protomers are recruited to the VRO by 2CATPase (the white boxes). Five protomers associate to form a single pentamer. This pentamer can then associate with viral RNA, which also binds to the VRO surface. B) Diagram of capsid formation. To form mature virions, pentamers bind RNA. The model assumes linear pentamer association. A group of 12 pentamers and RNA represents a mature virion. The left side of the panel (i) shows the process without the number of contact points of pentamer association being taken into account. The right side of the panel (ii) shows the process with the number of contact points being considered. Here, the white pentamers show that when three pentamers come together, the third pentamer can have either one (orange) or two contacts (red).

compared to 37°C[6]. However, none of the model simulations at 33°C resulted in a sustained prediction of higher virion production at 33°C in relation to that at 37°C. While some simulations had points where the expected virion concentration at 33°C was predicted to be higher than that at 37°C (Figure 3), this was not true at the endpoint of infection. Therefore, temperature-dependence alone is not sufficient to explain the unique temperature-dependent behavior of HRV infection. Thus, it became clear that other

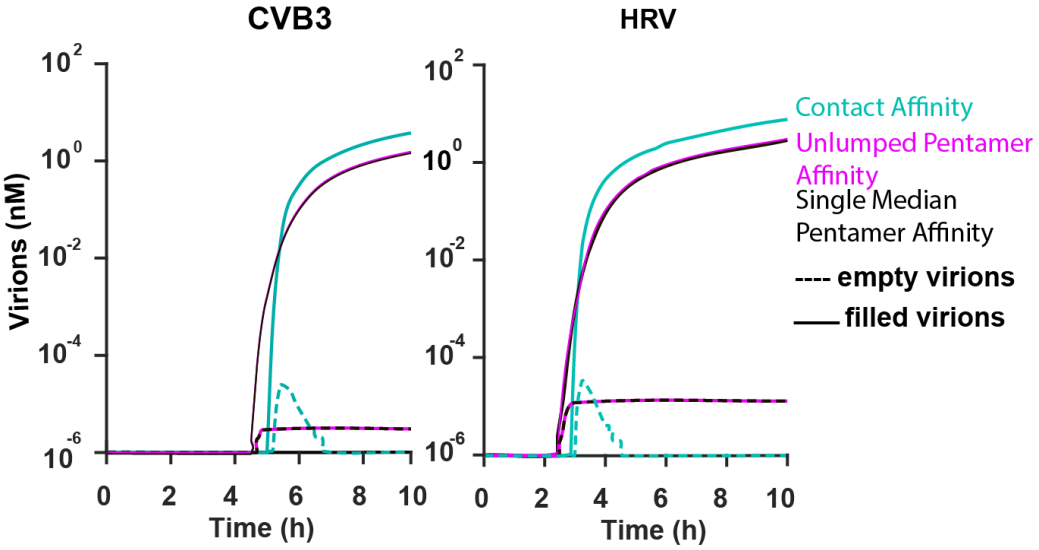

Figure 5: Effect of encapsidation module restructuring. Encapsidation module restructuring was done in one of two ways: either one new affinity value was used (single median pentamer affinity) or 12 new affinity values were used (unlumped pentamer affinity). The changes were compared to model predictions at the original affinity constant value (contact affinity). The modifications were made in both the CVB3 model and the HRV model at 37°C. Both graphs are on a log-linear scale.

judicious model changes might be necessary to capture temperature-dependent behavior.

Reevaluating encapsidation module assumptions

After concluding that temperature-dependence alone was insufficient to explain HRV's temperature-dependent behavior, we restructured the encapsidation module. Encapsidation is the process of encasing viral RNA into viral capsid proteins to form new virions to spread infection. The process begins with a translated polyprotein being cleaved into three capsid proteins (VP0, VP1, and VP3). These capsid proteins bind together to form a protomer. Next, five protomers come together to create a pentamer. Pentamers are recruited to the VRO by $2C^{ATPase}$. This process occurs at the viral replication organelle (VRO), which is an organelle composed of lipids stolen from host cell organelles and used as a factory to produce virions[15]. The creation of the VRO allows for efficient viral genome replication as it brings viral species into close proximity. This increases the local concentration of the viral species, which increases the amount of virus replicated to form new virions (Figure 4A). Pentamers on the VRO associate with other pentamers and viral RNA, which will allow them to eventually form mature virions (Figure 4A)[16].

Then, 12 pentamers assemble to form a capsid. The capsid must contain viral RNA to form an infectious virion. The model assumes that capsids form one pentamer at a time. The previous model uses the contact affinity, which describes the strength of association of any two pentamers coming together at a single contact point, as the affinity constant for all pentamers binding[11]. In reality, the affinity is dependent on the number of contacts that the new pentamer has. Depending on the number of pentamers already assembled, it is possible for a pentamer to have more than one contact (Figure 4B). Therefore, there is significant heterogeneity in the affinity between pentamers binding across different geometries. The encapsidation module was first restructured in the CVB3 model as this model has been published. Therefore, the effects of restructuring encapsidation could be verified against a validated model so that any changes in model predictions could be attributed solely to changes in encapsidation. The median pentamer affinity, which takes into account every possible geometry of pentamer formation and its associated affinity, was used in restructuring the encapsidation module. After applying this adaptation to the CVB3 model, the same conditions were applied to the HRV model. The same trends occurred in both CVB3 and HRV, confirming that the trends seen in HRV are due solely to the changes in the encapsidation module, and not other perturbations (Figure 5).

Two types of median pentamer affinities were applied to the model. In one case, a single median pentamer affinity was used. The filled virions curve of the single median pentamer affinity graph was very similar to that of the contact affinity curve in shape; however, the output of the single median pentamer affinity condition at 10 hours was approximately half that of the contact affinity condition (Figure 5). The same trend resulted when the changes were applied to the HRV model. When looking at the empty virions curve, the concentration of empty virions increases rapidly and then decreases back down to the baseline within a 5-hour timescale for both the original CVB3 and the HRV models using the contact affinity. However, with the single

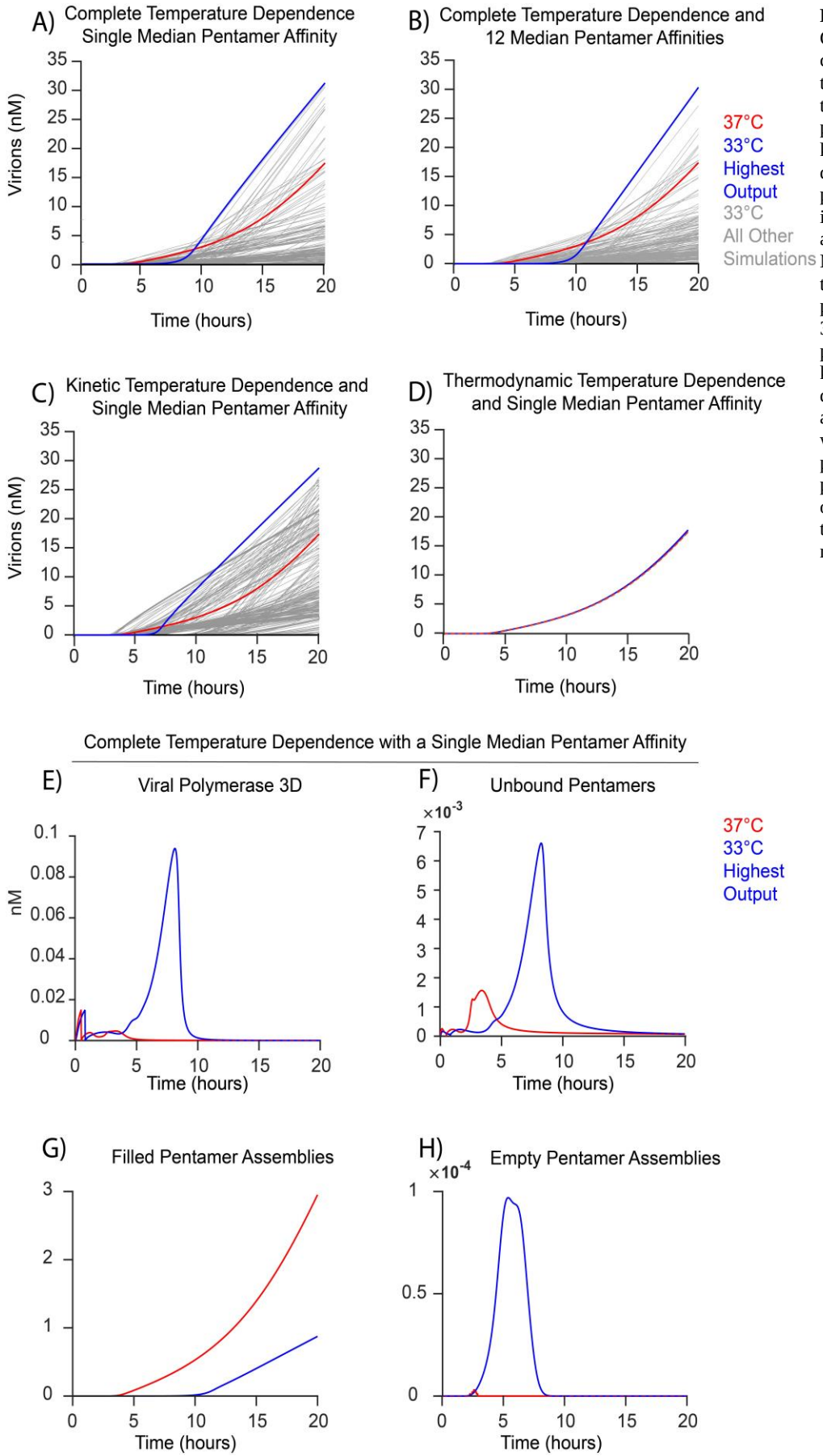

Figure 6: Temperature and Dependence and Geometric Encapsidation: A) Virion concentration predictions from the model that incorporates kinetic and thermodynamic temperature-dependence and a single median pentamer affinity B) Model that incorporates kinetic and thermodynamic temperature-dependence and 12 unlumped median pentamer affinities C) Model that incorporates kinetic temperature-dependence and a single median pentamer affinity D) Model that incorporates thermodynamic temperature-dependence and a single median pentamer affinity E and F) Viral polymerase 3D and viral protease concentration predictions from the model that incorporates kinetic and thermodynamic temperature-dependence and a single median pentamer affinity G) Concentrations of filled capsids which are pentamer assemblies that contain positive RNA but do not have a full 12 pentamers to form a virion H) Concentrations of empty capsids are pentamer assemblies that do not yet contain positive RNA and do not have a full 12 pentamers to form a virion

median pentamer affinity version of the model, it is predicted that the empty virion concentration approaches a nonzero steady state (Figure 5). This was not predicted by the original model and therefore represents a new predicted behavior.

In the second case, unlumped median pentamer affinities were used. This resulted in the use of 12 separate affinities, each of which represented the affinity of a different number of pentamers joining together. For example, there were separate affinities for the third pentamer binding and the fourth pentamer binding. The predictions generated by the unlumped median pentamer affinities condition were nearly identical to those generated by the single pentamer affinity model (Figure 5). This indicates that unlumping affinities within the encapsidation module is an unnecessary level of detail as it does not result in new model predictions.

Incorporation of temperature-dependence and new encapsidation assumptions

Next, four versions of the model incorporating various forms of temperature-dependence and encapsidation were compared. The first modeling condition included both kinetic and thermodynamic temperature-dependence and used a single median pentamer affinity that accounted for assembly geometry (Figure 6A). Incorporating both temperature-dependence and an updated affinity resulted in new temperature-dependent behavior, with 79% more virions at 20 hours at 33℃ than at 37℃. The switch to a single median pentamer affinity from a contact affinity (Figure 3) was essential to capture the temperature-dependence that results in higher virion production at lower temperatures.

The second condition included both kinetic and thermodynamic temperature-dependence and used twelve separate encapsidation parameters corresponding to each pentamer addition to the capsid (Figure 6B). Although unlumping the temperature-dependent parameters did not result in different model predictions compared to a single median pentamer affinity (Figure 5), we were interested to see if this trend continued at 33℃. Unlumping the median pentamer affinities resulted in 79% more virions at 20 hours at 33℃ than at 37℃. We concluded that unlumping does not change the model predictions about virion production and is an unnecessary layer of complexity for our purposes.

The third model condition incorporated only kinetic temperature-dependence, corresponding to rates within the delivery and replication module, and used a single median pentamer affinity (Figure 6C). This scenario similarly resulted in 76% more virions at 20 hours at 33℃ than at 37℃, demonstrating that kinetic temperature-dependence and using a single median pentamer affinity are sufficient to reveal more virion production at lower temperatures. This model lacked thermodynamic temperature-dependence, which alters rates within the encapsidation module, but still exhibited thermodynamic behavior. Thus, temperature-dependence within the encapsidation module is not necessary to reveal temperature-dependent behavior.

The fourth model condition included only thermodynamic temperature-dependence and used a single median pentamer affinity that accounted for assembly geometry (Figure 6D). In this condition, very little difference was observed in HRV infection at 33℃ in comparison to 37℃. Thus, thermodynamic temperature-dependence is not sufficient to reveal temperature-dependent behavior. Rather, kinetic temperature-dependence is critical for increased virion production at lower temperatures.

We investigated intermediates within the viral life cycle to determine when during infection the difference between 33℃ and 37℃ begins to emerge. All observations were made with the model condition of incorporating both kinetic and thermodynamic temperature-dependence and using a single median pentamer affinity. Within the delivery module, kinetic parameters sped up at 37℃, leading to quicker internalization. However, within the replication module, faster kinetic parameters did not necessarily lead to higher concentrations of each intermediate. At 33℃, viral infection steals a larger proportion of the host ribosomes for viral translation, which could be due to a reduced capacity of the host cells to defend against viral mechanisms at 33℃. This reduced defense capacity is seen in lower cleavage rates of viral proteins by the host cell so that the viral machinery is able to steal more ribosomes. There are also differences in the model predictions about the concentration of viral polymerase 3D over the course of infection. At 33℃, the polymerase 3D concentration continuously increases until it peaks around 7 hours (Figure 6E). Conversely, at 37℃, the polymerase 3D concentration peaks in the first hour, remains at a low level, and returns to zero by 5 hours (Figure 6E). The increase in viral polymerase leads to more transcription and the increase in viral ribosomes corresponds to more viral translation later in infection at 33℃, which is possibly an explanation for how more virions are produced at 33℃. A later peak of polymerase 3D could be due to the decrease in degradation rates at lower temperatures. At 33℃ the concentration of unbound pentamers within the viral replication organelle peaks at approximately 8 hours and has a maximum concentration of 6.5e-3 nM (Figure 6F). In comparison, at 37℃ the concentration of unbound pentamers within the viral replication organelle peaks at approximately 4 hours,

degradation rates and the increase in viral transcription at 33℃ could explain the increase in concentration of viral pentamers at 33℃. All other intermediates within the replication module had similar or lower concentrations at 33℃ in comparison to 37℃.

Within the encapsidation module, filled pentamer assemblies, which are pentamer assemblies of less than 12 pentamers containing positive RNA, were present in higher concentrations at 37℃ compared to 33℃ (Figure 6G). In contrast, empty pentamer assemblies, which are pentamer assemblies of less than 12 pentamers that have not yet bound positive RNA, have a higher concentration at 33℃ than 37℃ (Figure 6H). It is possible that the higher empty pentamer assembly concentration and viral polymerase concentration (corresponding to more viral RNA transcription) at 33℃ lead to more available intermediates for capsid assembly during encapsidation. This would lead to many empty pentamer assemblies binding to RNA later in infection, resulting in overall more total virions at later time points. The early peak in pentamers at 37℃ degrees (Figure 6F) corresponds to a smaller pentamer pool later in infection, which may correspond to many pentamer assemblies of less than 12 that cannot bind any additional pentamers to form a full capsid.

Both kinetic temperature-dependence and using a single median pentamer affinity are required within the model to reveal temperature-dependence that agrees with the observed temperature-dependence in HRV. Our model predictions point to the imbalance of viral intermediates at 37℃ as a possible mechanistic explanation for increased virion production at 33℃ as compared to 37℃.

Discussion

HRV infection begins faster but slows down due to imbalances in intermediates

We expected that the model would predict HRV virions appearing earlier than CVB3 virions, because the dissociation constant is lower for HRV than for CVB3. A low dissociation constant indicates a high affinity, so the binding of HRV with the receptor should be stronger than CVB3 binding to its receptor. Thus, HRV virions would begin being internalized faster. This is precisely what the model predicted which supported that model architecture was changed appropriately (Figure 2).

An unexpected result was that despite HRV virions appearing earlier than CVB3 virions, the slope of change in CVB3 virions over time was higher than that of HRV virions over time. This allowed for the CVB3 virion concentration to surpass that of HRV at approximately the 7-hour time point (Figure 2). This behavior is not expected because HRV has a faster internalization rate than CVB3. However, it is likely that the increased rate of delivery for HRV leads to various life-cycle intermediates rapidly being built up and then degraded by the host cell. This would lead to rate mismatches between the different lifecycle modules. This leads to the rate of virion production slowing at later points in HRV, as intermediates are degraded before they can be used to form new mature virions.

Incorporation of temperature-dependence leads to different viral intermediate behavior

At higher temperatures, kinetic rates will speed up. Thus, the rate at which virions are internalized should be higher at 37℃ than at 33℃. Therefore, we hypothesized that virions would appear sooner at 37℃ than 33℃, even if the virion concentration at 33℃ eventually surpassed that at 37℃. While some model simulations confirmed this hypothesis, others did not (Figure 3, 6A, 6B). However, it is important to note that model simulations that resulted in the expected behavior of virion production being higher at 33℃ also confirmed the hypothesis that virion internalization begins sooner at 37℃. Some combinations of enthalpy and activation energy values resulted in virions being internalized at the same time or even earlier at 33℃ when compared to 37℃; however, these simulations did not result in the overall expected trend. This is likely because faster internalization leads to viral intermediates being used up too rapidly or being degraded before they can be used. This imbalance of rates is apparent in the replication and encapsidation intermediates (Figure 6E,F) and leads to a decrease in new virion production.

An interesting trend in viral polymerase 3D was observed when looking at model intermediates. Viral polymerase 3D is necessary for the replication of viral RNA[17]. Therefore, since the concentration of viral polymerase 3D decreases so early on at 37℃, the model predicts that viral transcription quickly slows at 37℃ (Figure 6E). This trend is opposite at 33℃, where the concentration of viral polymerase steadily increases for a majority of the infection. This allows for transcription to continue to increase over the course of infection leading to a steadier rate of viral RNA production that peaks at a higher value. The lower levels of viral polymerase at 37℃ could potentially be explained by research indicating that at higher temperatures interferon (IFN) and interferon-stimulated gene (ISG) expression is higher. Both of these immune system components work to prevent HRV replication[8]. Therefore, this could lead to the lower levels of viral polymerase at 37℃ predicted by the model.

Also of importance is the different trends in concentration of unbound pentamers between 37℃ and

33°C. Unbound pentamers are necessary for the formation of capsids which can then form mature virions. Since unbound pentamer concentration spikes so early on at 37°C and then decreases for the remainder of infection, free pentamers are being consumed quickly. Moreover, at 37°C the pentamer degradation rate is also faster which further contributes to this rapid decrease in free pentamer concentration (Figure 6F). With low levels of free pentamers, virion production is not able to occur as rapidly, resulting in a lower overall concentration of virions. Contrastingly, the free pentamer concentration has a higher peak that is approximately 5 hours later at 33°C. This allows for a steady concentration of free pentamers that in turn can form capsids and result in a higher overall virion concentration.

Taking pentamer geometry into account is necessary for an explanation of greater virion production at lower temperatures

In regards to encapsidation module restructuring, we found that models that took into account pentamer formation geometry resulted in higher virion production at 33°C compared to 37°C (Figure 6A,B). This is likely attributable to the fact that pentamer contacts exert a large effect on the magnitude of the affinity constant. Specifically, a greater number of pentamer contacts results in a much stronger affinity. Therefore, by taking into account that pentamers can have up to 5 contacts, the affinity constant was made dramatically higher. This likely resulted in a more accurate characterization of pentamer behavior which in turn resulted in the previously documented trend of higher pentamer concentration at 33°C than 37°C. However, we found that the unlumped model, which included 12 separate median pentamer affinities, was no different from the model with only one overall median pentamer affinity (Figure 5). This indicated that unlumping encapsidation into multiple affinities was an unnecessary level of detail. This finding can be explained by the fact that the Van't Hoff equation for temperature-dependence that is applied to the encapsidation module was not necessary for predicting an increase in virion production at 33°C when compared to 37°C. Small alterations to the parameters used in the Van't Hoff equation due to unlumping then wouldn't affect model predictions either. This can explain why model predictions are nearly identical when 12 median pentamer affinities are used to when a single median pentamer affinity is used. In both cases, pentamer assembly geometry was considered, so the majority of the 12 pentamer affinities do not differ greatly from the single median pentamer affinity. In combination with the fact that the Van't Hoff equation does not affect model behavior predictions, this can explain why unlumping encapsidation into 12 separate affinities proved unnecessary.

Both the single median pentamer affinity model and the unlumped pentamer affinity model result in the prediction of the formation of a stable population of empty provirions (Figure 5). This is not predicted by the original CVB3 model. This new finding can be explained by the fact that the affinity constant for pentamer binding is much stronger when pentamer geometries of formation are taken into account. Therefore, pentamer bonds with one another are more stable. As a result, pentamers are able to form stable groups readily, but the limiting factor appears to be viral RNA binding. The production of viral RNA is directly affected by the concentration of viral polymerase 3D, which is not constant in either the 37°C or the 33°C case. With strong pentamer association and variable levels of viral RNA, mature virion production likely cannot occur as quickly as capsids are being formed. Thus, a stable concentration of provirions remains empty over the course of infection as opposed to the quick decrease in empty provirion concentration predicted in the original CVB3 model.

Limitations and Future Work

A limitation of our model is that we used several estimates or proxies for uncharacterized parameters, both within the delivery module and with encoding temperature-dependence. Many of the parameters within the delivery module were not sensitive to doubling or halving, so estimates are appropriate and do not greatly affect the model predictions. However, plausible ranges were also used for some of the more sensitive parameters, including the activation energies and enthalpies. Our model shows that it is possible for HRV temperature-dependence to be kinetically modeled, if the biological parameters match the activation energy and enthalpy estimates we used. Our model would be more conclusive if direct biological measurements existed to replace our estimates for the unknown parameters. As an alternative, we could experimentally calculate unknown parameters related to binding and internalization. Similarly, we could experimentally determine if there is a stable population of empty virions at 33°C as was predicted by the change in encapsidation module assumptions to further validate our model predictions.

A further limitation is that the encapsidation module still contains simplifications. One assumption in our model is that capsid assembly occurs linearly, with one pentamer added at a time. However, biologically we know that groups of pentamers can join together in non-linear assembly. The extent of how changing this assumption

would affect the model predictions was not thoroughly investigated by our model. While encoding every possible path of non-linear pentamer assembly would be computationally restrictive, it may be possible to calculate the binding affinities for all of the possible pentamer assembly formations, including pathways of non-linear assembly, and calculate a single weighted median. We show that using a single weighted median for all twelve linear pentamer binding affinities is a simplification that does not change model predictions, so future work could investigate if using a similar approach to incorporate non-linear encapsidation changes the model behavior.

Our model shows several combinations of biologically plausible activation energies and enthalpies that lead to temperature-dependent behavior. However, it is possible that these values are not biologically accurate for HRV infection, and some other mechanism is responsible for HRV's unusual temperature-dependent behavior that was not captured by our model. Future work could experimentally determine what that activation energies and enthalpies for each reaction are. Obtaining the experimental values for activation energy and enthalpy would confirm if the activation energies and enthalpies predicted by our model are accurate.

Materials and Methods

Adapting the model to HRV

Past iterations of the model use a series of differential equations to track the total concentration of various biomolecules throughout the viral life cycle[11]. To change the delivery module to reflect the receptor binding and internalization of HRV, new reaction rates were calculated and a new series of differential equations were created (S2,3). ICAM is used as the example here, but the same formula structures apply for LDLR. These new differential equations require new parameters: the binding and dissociation rates of HRV with both its major (ICAM) and minor (LDLR) receptors and the rate of endocytic internalization (S1). These kinetic rates were all calculated or estimated from literature and compared to other biologically similar interactions to check that they are biologically feasible. Some rates were estimated using rates from other similar reactions. For example, the binding affinity of HRV2 to LDLR is not characterized, however the binding of LDLR to other similarly sized molecules, like Low Density Lipoprotein (LDL), is. This rate was used as a proxy for the HRV2-LDLR interaction. Our confidence in this rate was supported by the similar behavior of HRV2 and HRV3 (Figure 2). Results from the model were compared to available kinetic data to verify the model's accuracy. A Multiplicity of Infections (MOIs) of 10 was used for all comparisons, as this was the most common MOI found in the literature.

Incorporation of temperature-dependence

Temperature-dependence was incorporated into the model through the application of two unique temperature-dependent equations. For the delivery module and eplication module, which computationally represent enzymatically driven processes, a kinetic temperature-dependent equation was used. Specifically, the Arrhenius equation,

$$k = Ae^{\frac{-E_a}{RT}} \quad [1]$$

where k is the rate constant (1/hr), A is the preexponential factor (1/hr), E_a is the activation energy (cal/mol), R is the ideal gas constant (1.98558 cal/mol/K), and T is the temperature in kelvin, was used. To use this equation, the temperature was changed from 310 K (37°C) to 306 K (33°C). We compared model predictions at both 33°C and 37°C. Given that all the rate constants were initially defined at 37°C, the rate constants at 33°C were of particular interest. To determine the value of these constants at the new temperature, activation energies for each of the kinetic parameters in the model were necessary. A sensitivity analysis was performed in which each parameter was changed 2 fold in both directions. Thus was done as it was assumed that temperature changes within physiological ranges would not realistically change a parameter by more than 100%. If a two-fold change resulted in less than 10% change in downstream measures, it was not a sensitive parameter, and would not be included in temperature-dependence. The sensitivity analysis revealed 25 sensitive parameters. Of these 25 parameters, 7 parameters had specific activation energies that were characterized in literature (S4). For the remaining 18, a range of biologically plausible activation energies was chosen. For each simulation of the model, the model chose between 2,000 cal/mol, 20,000 cal/mol, and 200,000 cal/mol for each of the unknown parameters resulting in a large number of possible combinations of activation energies.

For the encapsidation module, which computationally represents processes driven by self-assembly and bond formation, a thermodynamic temperature-dependent equation was used. Specifically, the Van't Hoff equation,

$$\ln\left(\frac{k_2}{k_1}\right) = -\frac{\Delta H^\circ}{R}\left(\frac{1}{T_2} - \frac{1}{T_1}\right) \quad [2]$$

where k_2 is the new affinity constant (1/hr), k_1 is the original affinity constant (1/hr), ΔH° is the standard enthalpy of the reaction (cal/mol), R is the ideal gas constant (1.98558 cal/mol/K), T_1 is the original temperature (K), and T_2 is the new temperature (K), was used. The Van't Hoff equation was applied to the affinity constant parameters in the model. The rates for these parameters were originally

defined at 37℃. Thus, the rates were recalculated at 33℃ for comparison. To do so a range of biologically plausible standard enthalpy values was determined based on a literature search. For each model simulation, one of the 9 enthalpies between -50,000 cal/mol and 50,000 cal/mol was chosen.

Both the Arrhenius equation and the Van't Hoff equation were applied to the model simultaneously. Approximately 3,000 model simulations were run each time results were collected. In each of the 3,000 simulations, the model randomly chose an activation energy and enthalpy value within the defined range for each of the unknown parameters. The goal was to identify possible combinations of activation energies and enthalpies that resulted in the expected model behavior, which was virion production being higher at 33℃ than 37℃.

Encapsidation Module Restructuring

The encapsidation module was restructured so geometry was taken into account with pentamer association. To do so, the "Capsid Affinity Script" published by Endres and Zlotnick was used[20]. This code outputs the dissociation constants associated with each pentamer addition and the corresponding number of contacts that the new pentamer had to another pentamer (S5). The affinity can then be calculated as the inverse of the dissociation constant. Originally, the model used the contact affinity of 1e3 nM as the affinity for all pentamers joining together which did not account for the effects of geometry of assembly. The affinity constant was then recalculated in one of two ways. First, the overall median pentamer affinity was found by taking the weighted median of all the values in the table. This represented the affinity associated with all possible geometries of capsid formation. The affinity constant in this case was 2.58e-6 nM. Second, the affinity for each number of pentamers coming together was found. This resulted in 12 separate affinity constants, identified in the last row of Supplementary Table 5. Each affinity constant represented the weighted median affinity of the possible geometries associated with that pentamer addition. This required the encapsidation module to be unlumped so that there were 12 different equations for pentamer association and dissociation where each was defined by a different affinity constant.

End Matter

Author Contributions and Notes

P.C.M, M.C.P, and A.S wrote code; P.C.M and M.C.P performed literature searches; P.C.M, M.C.P, K.A.J, and A.S interpreted data; P.C.M and M.C.P wrote the paper.
The authors declare no conflict of interest.

Acknowledgments

We would like to thank Kevin Janes, Ph.D. and Andrew Sweatt from the U.Va Department of Biomedical engineering for their guidance throughout the duration of this project.

References

1. Mohamud, Y. & Luo, H. The Intertwined Life Cycles of Enterovirus and Autophagy. Virulence 10, 470–480 (2018).
2. Factsheet about enteroviruses. European Centre for Disease Prevention and Control https://www.ecdc.europa.eu/en/enteroviruses/facts.
3. Garmaroudi, F. S. et al. Coxsackievirus B3 replication and pathogenesis. Future Microbiol. 10, 629–653 (2015).
4. Jacobs, S. E., Lamson, D. M., St. George, K. & Walsh, T. J. Human Rhinoviruses. Clin. Microbiol. Rev. 26, 135–162 (2013).
5. Hung, I. F. N. et al. Unexpectedly Higher Morbidity and Mortality of Hospitalized Elderly Patients Associated with Rhinovirus Compared with Influenza Virus Respiratory Tract Infection. Int. J. Mol. Sci. 18, (2017).
6. Papadopoulos, N. G., Sanderson, G., Hunter, J. & Johnston, S. L. Rhinoviruses replicate effectively at lower airway temperatures. J. Med. Virol. 58, 100–104 (1999).
7. Blaas, D. & Fuchs, R. Mechanism of human rhinovirus infections. Mol. Cell. Pediatr. 3, (2016).
8. Foxman, E. F. et al. Temperature-dependent innate defense against the common cold virus limits viral replication at warm temperature in mouse airway cells. Proc. Natl. Acad. Sci. U. S. A. 112, 827–832 (2015).
9. Yin, J. & Redovich, J. Kinetic Modeling of Virus Growth in Cells. Microbiol. Mol. Biol. Rev. MMBR 82, (2018).
10. Sidorenko, Y. & Reichl, U. Structured model of influenza virus replication in MDCK cells. Biotechnol. Bioeng. 88, 1–14 (2004).
11. Lopacinski, A. B. et al. Modeling the complete kinetics of coxsackievirus B3 reveals human determinants of host-cell feedback. Cell Syst. 12, 304-323.e13 (2021).
12. Egilmez, H. I. et al. Temperature-dependent virus lifecycle choices may reveal and predict facets of the biology of opportunistic pathogenic bacteria. Sci. Rep. 8, 9642 (2018).
13. Organtini, L. J., Makhov, A. M., Conway, J. F., Hafenstein, S. & Carson, S. D. Kinetic and Structural Analysis of Coxsackievirus B3 Receptor Interactions and Formation of the A-Particle. J. Virol. 88, 5755–5765 (2014).

14. Casasnovas, J. M. & Springer, T. A. Kinetics and Thermodynamics of Virus Binding to Receptor. STUDIES WITH RHINOVIRUS, INTERCELLULAR ADHESION MOLECULE-1 (ICAM-1), AND SURFACE PLASMON RESONANCE. J. Biol. Chem. 270, 13216–13224 (1995).
15. Hsu, N.-Y. et al. Viral Reorganization of the Secretory Pathway Generates Distinct Organelles for RNA Replication. Cell 141, 799–811 (2010).
16. Ma, H.-C. et al. An Interaction between Glutathione and the Capsid Is Required for the Morphogenesis of C-Cluster Enteroviruses. PLOS Pathog. 10, e1004052 (2014).
17. Nirwan, S. & Kakkar, R. Rhinovirus RNA Polymerase. Viral Polym. 301–331 (2019) doi:10.1016/B978-0-12-815422-9.00011-5.
18. Endres, D. & Zlotnick, A. Model-based analysis of assembly kinetics for virus capsids or other spherical polymers. Biophys. J. 83, 1217–1230 (2002).
19. Rankl, C. et al. Multiple receptors involved in human rhinovirus attachment to live cells. Proc. Natl. Acad. Sci. U. S. A. 105, 17778–17783 (2008).
20. Mathematical Model for Low Density Lipoprotein (LDL) Endocytosis by Hepatocytes | SpringerLink. https://link.springer.com/article/10.1007/s11538-008-9347-9.
21. Weigel, P. H. & Oka, J. A. Temperature dependence of endocytosis mediated by the asialoglycoprotein receptor in isolated rat hepatocytes. Evidence for two potentially rate-limiting steps. *J. Biol. Chem.* **256**, 2615–2617 (1981).
22. Craig, N. Regulation of translation in rabbit reticulocytes and mouse L-cells; comparison of the effects of temperature. *J. Cell. Physiol.* **87**, 157–166 (1975).
23. Kellenberger, E. DNA viruses: cooperativity and regulation through conformational changes as features of phage assembly. *Philos. Trans. R. Soc. Lond. B. Biol. Sci.* **276**, 3–13 (1976).
24. Craig, N. Effect of temperature on protein and immunoglobulin synthesis and secretion in two mouse myeloma cell lines. *J. Cell. Physiol.* **100**, 323–334 (1979).
25. Gindulyte A, Bashan A, Agmon I, Massa L, Yonath A, Karle J. The transition state for formation of the peptide bond in the ribosome. Proc Natl Acad Sci U S A. 2006;103(36):13327-32. Epub 2006/08/30. doi: 10.1073/pnas.0606027103. PubMed PMID: 16938893; PMCID: PMC1557383.

Supplementary Material

	HRV2-LDLR	HRV3-ICAM1	CVB3
Receptor Binding (M-1s-1)	2e5[19]	6100 (First Binding Site)[14] 975 (Second Binding Site)[14]	1.47e5 (Coreceptor)[11] 3.35e3 (Receptor)[11]
Receptor Dissociation(s-1)	5e-7[19]	1.8e-3 (First Binding Site)[14] 1.95e-3 (Second Binding Site)[14]	0.3 (Coreceptor)[11] 8.21e-4 (Receptor)[11]
Virion Internalization(hr-1)	16.56[20]	3.2[14]	0.5[11]

Supplemental Table 1: Enterovirus binding and internalization parameters. Receptor binding is the rate at which the virus binds to its receptor. Receptor dissociation is the rate at which the receptor-virus complex dissociates. Viral Internalization is the rate of internalization, where the bound virus is taken up by the cell.

Supplement Table 2: Rate Equations
ICAMform = k_on_ICAM * uHRV * uICAM
ICAMdiss = k_off_ICAM * bICAM
Internalization = k_internal * bICAM
RNARelease = k_endo_escape * +RNA_endo
Supplementary Table 2: Rate equations. ICAMform is the rate at which HRV-bound ICAM forms. ICAMdiss is the rate at which this complex dissociates. Internalization is the rate at which the HRV-ICAM complex is endocytosed. uHRV is unbound HRV, uICAM is unbound ICAM and bICAM is bound ICAM.

$$\frac{d[uHRV]}{dt} = [bICAM] * K_{off} - [uHRV] * [uICAM] * K_{on}$$

$$\frac{d[uHRV_{Defective}]}{dt} = [bICAM_{Defective}] * K_{off} - [uHRV_{Defective}] * [uICAM] * K_{on}$$

$$\frac{d[uICAM]}{dt} = ([bICAM] + [bICAM_{Defective}]) * K_{off} - ([uHRV] + [uHRV_{Defective}]) * [uICAM] * K_{on} + ([bICAM] + [bICAM_{Defective}]) * K_{int}$$

$$\frac{d[bICAM]}{dt} = [uHRV] * [uICAM] * K_{on} - [bICAM] * (K_{off} + K_{int})$$

$$\frac{d[bICAM_{Defective}]}{dt} = [uHRV_{Defective}] * [uICAM] * K_{on} - [bICAM_{Defective}] * (K_{off} + K_{int})$$

$$\frac{d[+RNA_{Endosomal}]}{dt} = [bICAM] * K_{int} * InternalVolumeConversion - [+RNA_{Endosomal}] * K_{RNARelease}$$

$$\frac{d[+RNA_{EndosomalDefective}]}{dt} = [bICAM_{Defective}] * K_{int} * InternalVolumeConversion - [+RNA_{EndosomalDefective}] * K_{RNARelease}$$

Supplementary Table 3: Differential equations. uHRV is unbound HRV, uICAM is unbound ICAM, bICAM is bound ICAM, and +RNA_endo is positive ssRNA within the endosome. Non-infectious viral particles are represented by uHRV_Defective, and other Defective equations are included to account for the complexes and endosomes formed with these non-infectious particles.

Parameter	Activation Energy	Reference
Kinternal (rate of internalization)	17.0 kcal/mol	[21]
K_t_c_form (translation complex formation)	12 kcal/mol	[22]
K_translate (rate of translation and complex dissociation)	12 kcal/mol, 24 kcal/mol (two sources)	[22]
K1b_cap (empty proviron dissociation)	247 kJ/mol	[23]
kRNACapUnbind (provirion dissociation)	247 kJ/mol	[23]
u_ISG (degredation of ISG in cytoplasm)	22 kcal/mol	[24]
ISGFormRate (rate of ISG formation)	18 kcal/mol	[25]

Supplemental Table 4: Activation energies for sensitive model parameters. After completing a sensitivity analysis, a literature search was done to characterize the activation energies of rates deemed sensitive to model perturbations so that the Arrhenius equation could be applied. The activation energy for 7 sensitive parameters was obtained.

Supplemental Table 5: Dissociation constants (nM) for each combination of subunits and contacts

number of subunits	2	3	4	5	6	7	8	9	10	11	12
number of contacts											
1	0.0004	0.00195	0.00317	0.00399	0.00454	0.00492	0.00520	0.00541	0.00557	0.00569	0.00579
2	4.00E-07	1.10E-05	3.17E-05	5.32E-05	7.19E-05	8.75E-05	0.0001	0.00011	0.00012	0.00013	0.00013
3	NaN	6.16E-08	3.17E-07	7.09E-07	1.14E-06	1.56E-06	1.94E-06	2.28E-06	2.58E-06	2.85E-06	3.09E-06
4	NaN	NaN	3.17E-09	9.46E-09	1.81E-08	2.77E-08	3.74E-08	4.68E-08	5.57E-08	6.39E-08	7.14E-08
5	NaN	NaN	NaN	1.26E-10	2.86E-10	4.92E-10	7.22E-10	9.61E-10	1.20E-09	1.43E-09	1.65E-09
median KD	0.0002	1.095E-05	1.603E-05	7.092E-07	1.139E-06	1.556E-06	1.937E-06	2.279E-06	2.583E-06	2.852E-06	3.091E-06

Supplemental Table 5: Dissociation constants (nM) for each combination of subunits and contact. The number of subunits corresponds to the number of separate pentamers joining together. The number of contacts refers to the number of other pentamers the new pentamer being added is touching. A table value of NaN indicates that the corresponding number of contacts is not possible for that number of subunits. Each value indicates the dissociation constant associated with the corresponding number of pentamer subunits and contacts.